Mechanisms of Monovalent Cation Action in Enzyme Catalysis: The First Stage of the Tryptophan Synthase β-Reaction†

Eilika Woehl‡ and Michael F. Dunn*

Department of Biochemistry, University of California at Riverside, Riverside, California 92521

Received December 11, 1998; Revised Manuscript Received March 29, 1999

ABSTRACT: The tryptophan synthase bienzyme complex is activated and regulated by the allosteric action of monovalent cations (MVCs). The kinetic dissection of the first stage (stage I) in the β-reaction of tryptophan synthase, the reaction of L-serine with pyridoxal 5′-phosphate at the β-site to give the α-aminoacrylate Schiff base intermediate, E(A-A), is here examined in the absence and presence of MVCs. This analysis reveals which of the individual steps are greatly affected in stage I and how the ground states and transition states are affected by MVCs. Kinetic studies in combination with a detailed relaxation kinetic analysis to determine the specific rate constants for the conversion of the L-Ser external aldimine, $E(Aex_1)$, to E(A-A) show that the primary kinetic isotope effect for proton abstraction from Cα of the $E(Aex_1)$ species changes from 4.0 ± 0.4 in the absence of MVCs to a value of 5.9 ± 0.5 in the presence of Na^+, indicating that the nature of the transition state for this C−H scission is significantly perturbed by the MVC effect. The E(A-A) species was found to exist in two conformations with different activities, the ratio of which is affected by the presence of MVCs. It is shown that changes in the rate constants of stage I are important in establishing the ratio of active to inactive conformations of the E(A-A) species. Consequently, the MVC effect alters the relative energies of both the transition states and the ground states for selected steps in stage I of the pathway. Hence, interactions at the MVC site give rise to a fine-tuning of the covalent bonding interactions between active site residues and the reacting substrate during the conformational cycle of the bienzyme complex.

Within the past few years, it has become apparent that monovalent cation (MVC) activation/inhibition has evolved as a device used by a large number of enzymes to modulate catalysis and regulation (*1*). The list of enzymes known to be affected by MVCs is still growing. The definition of MVC binding sites by high-resolution X-ray techniques and solution studies on a few examples of monovalent metal ion activated enzymes has shown that MVCs generally act as allosteric effectors through specific binding interactions at a site separate from the catalytic site. Earlier work from our laboratory (*2*) and work by Peracchi et al. (*3*) have demonstrated that the tryptophan synthase bienzyme complex is subject to MVC activation. Our work showed that in the absence of metal ions both the activity is reduced and the allosteric cross-talk between subunits is lost. Recently, the structure of the MVC binding site in tryptophan synthase has been determined (*4*, *5*). Therefore, the bienzyme complex is an excellent paradigm for investigating the action of MVCs both in catalysis and in the allosteric regulation of substrate channeling (*6*).

The tryptophan synthase bienzyme complex from *Salmonella typhimurium* catalyzes the final two steps in the biosynthesis of tryptophan (*7*−*9*). The complex is of tetrameric subunit composition ($\alpha_2\beta_2$) with subunits arranged in an elongated $\alpha\beta\beta\alpha$ structure of ∼150 Å total length (*10*−*12*). A cartoon of the $\alpha\beta$-dimeric unit depicting some of the salient structural features of the complex is presented in Figure 1A. The α-subunit catalyzes the cleavage of IGP to G3P and indole (Scheme 1). The β-subunit catalyzes the condensation of indole with L-Ser to form L-Trp (Scheme 1). The overall process (conversion of IGP and L-Ser to L-Trp, G3P, and H_2O) is referred to as the $\alpha\beta$-reaction.

The β-reaction occurs in two stages (Scheme 1). In stage I, the first substrate of the β-reaction, L-Ser, reacts with the enzyme-bound PLP cofactor to form an α-aminoacrylate intermediate, E(A-A).[1] In stage II, this intermediate reacts with the second substrate, indole, to form L-Trp.

The $\alpha\beta$-dimer is the functional allosteric unit of the bienzyme complex (Figure 1). No allosteric interactions are

† Supported by NIH Grant GM55749 and NSF Grant MCB-9218902 (E.W.).

* Corresponding author. Phone: 909-787-4235. Fax: 909-787-4434. E-mail: michael.dunn@ucr.edu.

‡ Present address: Howard Hughes Medical Institute, School of Medicine, Yale University, New Haven, CT 06510.

[1] Abbreviations: $\alpha_2\beta_2$, the tryptophan synthase bienzyme complex; β_2, the β-subunit dimer; IGP, 3-indolyl-D-glycerol 3′-phosphate; 5-fluoro-IGP, the 5-fluoro derivative of IGP; IPP, 3-indolylpropanol 3′-phosphate; G3P, D-glyceraldehyde 3-phosphate; GP, α-glycerophosphate; L-Ser and D,L-Ser, L-serine and D,L-serine, respectively; L-Trp, L-tryptophan; PLP, pyridoxal 5′-phosphate; Bicine, *N*,*N*-bis(2-hydroxyethyl)glycine; KIE, kinetic isotope effect; SWSF single-wavelength stopped flow; RSSF, rapid-scanning stopped flow. The various covalent forms of PLP-bound serine at the β-site (see Scheme 1) are designated as follows: E(Ain), the internal aldimine (Schiff base); $E(GD_1)$, the first *gem*-diamine species; $E(Aex_1)$, the L-Ser external aldimine (Schiff base); $E(Q_1)$, the L-Ser quinonoid; E(A-A), the α-aminoacrylate Schiff base; $E(Q_2)$, the quinonoid formed initially in the Michael addition of indole with E(A-A); $E(Q_3)$, the quinonoid formed by abstraction of a proton from $E(Q_2)$; $E(Aex_2)$, the L-Trp external aldimine (Schiff base); $E(GD_2)$, the L-Trp *gem*-diamine; E(MK), the methyl ketoimine tautomer of E(A-A).

10.1021/bi982918x CCC: $18.00
Published on Web 05/11/1999

known to be transferred across the $\beta-\beta$ subunit interface of the holoenzyme. The active sites of neighboring α- and β-subunits are separated by about 25−30 Å and are connected by a tunnel (*12*, *13*), the preferential route of transfer for the common intermediate, indole, from the α-site to the β-site (*14*−*20*). A system of reciprocal allosteric interactions exerted through the $\alpha-\beta$ subunit interface ensures the coordination of the α- and β-reactions (*2*, *6*, *16*, *17*, *19*, *20*−*25*) (Figure 1). A key feature of this coordination involves the switching of $\alpha\beta$-dimeric units from an open conformation of low α-site activity to a closed conformation of high α-site activity in stage I, as depicted in Figure 1B.

In this work, we investigate the mechanism of MVC action on stage I of the tryptophan synthase β-reaction. It will be shown that the MVC effect acts to selectively alter both the ground-state stabilities of intermediates along the pathway and the activation energies of chemical steps in catalysis.

MATERIALS AND METHODS

Materials. L-Ser, indole, D-glyceraldehyde 3-phosphate (G3P) as the diethylacetal, and D,L-α-glycerophosphate (GP) were purchased from Sigma. Triethanolamine (TEA) was purchased from Aldrich as the base and adjusted to pH 7.8 with HCl. IGP was synthesized as previously described (*26*). After lyophilization, the remaining NH_4^+ ions were removed using a DEAE-Sephadex A-25 column in the H^+ form. IGP was loaded onto the column and, after thorough rinsing, eluted with 0.25 M TEA (pH 7.8). The [α-^{2}H]-L-Ser used in these studies was prepared by the *O*-acetylserine sulfhydrylase catalyzed stereospecific exchange of the α-^{1}H of L-Ser with ^{2}H of ^2H_2O (99.8% ^{2}H, Cambridge Isotopes). The *O*-acetylserine sulfhydrylase was a gift provided by Professor Paul Cook. The enzyme was removed by filtration through a 10 000 nominal molecular weight cutoff filter. The [α-^{2}H]-L-Ser was isolated by freeze-drying the filtrate, and the exchange was shown to be >98% by mass spectrometry. When assayed for activity in the tryptophan synthase β-reaction, no evidence of racemization was found. The [α-^{2}H,β-$^2H_2$]-D,L-Ser (98%) was purchased from Cambridge Isotopes.

Purification of tryptophan synthase from *S. typhimurium* was performed as previously described using plasmid pEBA-10 (*26*−*29*). The enzyme is stored in Bicine buffer containing monovalent metal ions and PLP. Prior to usage, the enzyme was dialyzed against metal-free TEA buffer (pH 7.8) to remove MVCs. All experiments reported in this paper were carried out at 25 °C in 50 mM TEA buffer at pH 7.80.

UV/Visible Absorbance Measurements and Activity Assays. Static UV/vis absorbance measurements were performed on a Hewlett-Packard 8452A diode array spectrophotometer. Direct photometric assays were used to measure the activity of the α-, β-, and $\alpha\beta$-reactions. The cleavage of IGP to indole and G3P was followed by measuring the decrease in absorbance at 290 nm ($\Delta\epsilon$ = 1.39 mM^{-1} cm^{-1}) (*30*). The conversion of indole to L-Trp was measured by the increase in absorbance at 290 nm ($\Delta\epsilon$ = 1.89 mM^{-1} cm^{-1}). The conversion of IGP to L-Trp was determined by measuring the increase in absorbance at 290 nm ($\Delta\epsilon$ = 0.56 mM^{-1} cm^{-1}).

Rapid-Scanning and Single-Wavelength Stopped-Flow Measurements. RSSF and SWSF measurements were performed as previously described (*31*−*36*). In each RSSF experiment, a set of 25 scans is collected, and subsets of these spectra are displayed in the figures shown herein. The following timing sequences identify the time points for the scans shown. Two different timing sequences are used. Timing sequence 1: 1 = 8.54 ms, 2 = 17.09 ms, 3 = 25.63 ms, 4 = 34.18 ms, 5 = 42.72 ms, 6 = 59.81 ms, 8 = 93.98 ms, 10 = 0.1282 s, 15 = 0.3845 s, 20 = 0.8544 s, and 25 = 1.7088 s. Timing sequence 2: 1 = 8.54 ms, 2 = 17.09 ms, 3 = 25.63 ms, 4 = 34.18 ms, 5 = 42.72 ms, 6 = 76.90 ms, 8 = 0.1452 s, 10 = 0.2136 s, 15 = 0.6408 s, 20 = 1.7088 s, and 25 = 4.2720 s. Single-wavelength time courses were fit by the Marquardt−Levenberg algorithm to equations of the general form:

$$A = A_\infty \pm \sum A_n \exp\left(\frac{-t}{\tau_n}\right) \qquad (1)$$

where *n* refers to the number of relaxations detected.

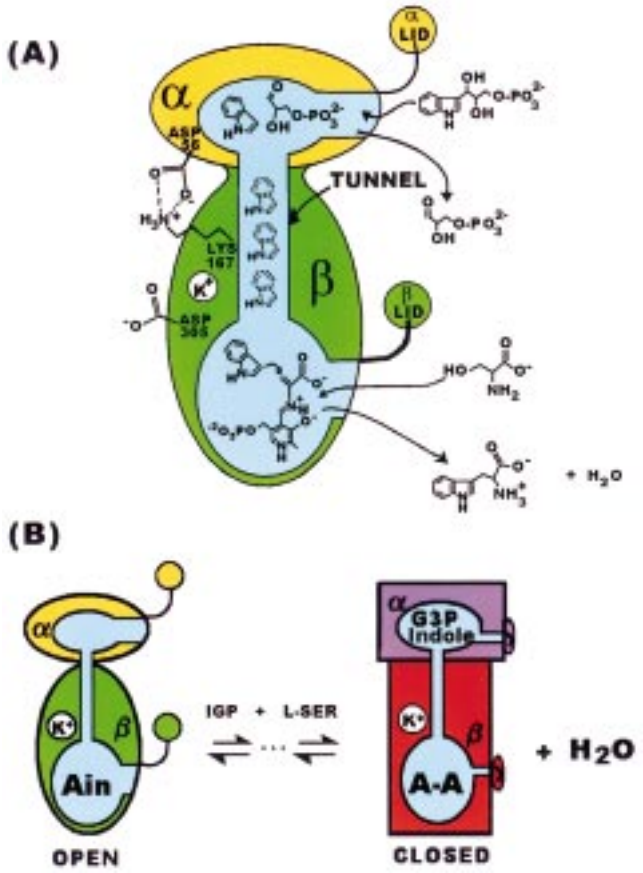

FIGURE 1: Cartoons showing the $\alpha\beta$-dimeric unit of the tetrameric tryptophan synthase bienzyme complex. (A) Cartoon depicting the active sites of the α- and β-subunits, the 25 Å long interconnecting tunnel, the entry of IGP and exit of G3P at the α-site, the diffusion of indole (dashed structures) through the tunnel into the β-site, the entry of L-Ser and exit of L-Trp, and a water molecule at the β-site. The β-site is shown occupied by the cleavage products, indole and G3P. The α-aminoacrylate derivative of PLP is shown undergoing nucleophilic attack by indole at the β-site. Components of the network of residues known to be involved in communicating allosteric signals between the α- and β-sites include the MVC site (shown occupied by K^+), βLys167 and αAsp56 (shown in a salt bridge), and βAsp305. Also shown are the "lids" which close down over the α- and β-sites to give closed structures. (B) Cartoon showing the switch from an open conformation to a closed conformation as E(Ain) is converted to the complex of E(A-A) with G3P and indole. Redrawn from Pan et al. (*6*) with permission.

Scheme 1: α- and β-Reactions[a]

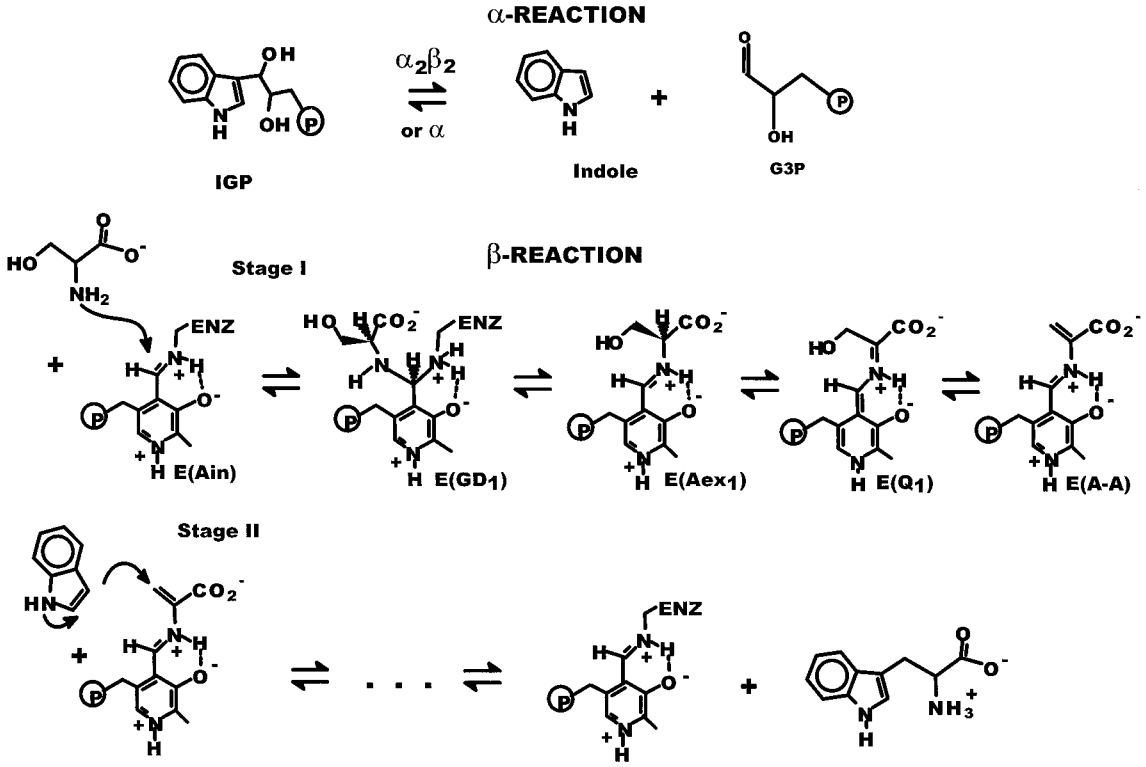

[a] Organic structures for the intermediates along the reaction path are shown for stage I of the β-reaction. The overall transformation corresponding to stage II is also indicated.

Kinetic Simulation Studies. Kinetic simulations of stage I of the β-reaction pathway were performed via the program Kinetic 3.11 (*37*).

RESULTS

Fluorescence and Single-Wavelength Absorbance Stopped-Flow Kinetic Analysis of the First Stage of the β-Reaction. In stage I of the β-reaction, the enzyme-bound PLP cofactor reacts with L-Ser to form an equilibrium mixture of intermediates dominated by the $E(Aex_1)$ and E(A-A) species (Scheme 1). To assess the MVC effect on individual kinetic parameters, this reaction was investigated under conditions of varying L-Ser concentrations in the absence and presence of NaCl (see Figures 2 and 3). The $E(Aex_1)$ species is the only highly fluorescent intermediate on the pathway (*38*, *39*). The intrinsic fluorescence of $E(Aex_1)$ is about 13-fold higher than that of the unbound enzyme, the only other species with significant fluorogenic properties. The fluorescence time course for appearance and decay of $E(Aex_1)$ was followed after the enzyme was rapidly mixed with different concentrations of L-Ser, both in the absence and in the presence of Na^+ (Figure 2). At higher L-Ser concentrations, there is a very rapid phase of $E(Aex_1)$ formation that is almost complete within the mixing dead time. The transiently accumulated $E(Aex_1)$ species then relaxes in a biphasic process to form an equilibrium mixture of $E(Aex_1)$ and E(A-A) species. In the presence of Na^+ ions, there is another, slower, increasing phase (about 50−100 s^{-1}) that seems to be independent of the L-Ser concentration. This phase could not be assigned. It might very likely stem from some of the less well understood conformational transitions in the complex. The ratio of the amplitude of that phase to the amplitude of the faster phase decreases with increasing L-Ser concentration, probably due to the increase in rate of the faster phase. The kinetic titration analysis was performed with both isotopically normal L-Ser and deuterated [α-^{2}H]-L-Ser to obtain information about intrinsic isotope effects for evaluation of the steady-state behavior of the system (see below).

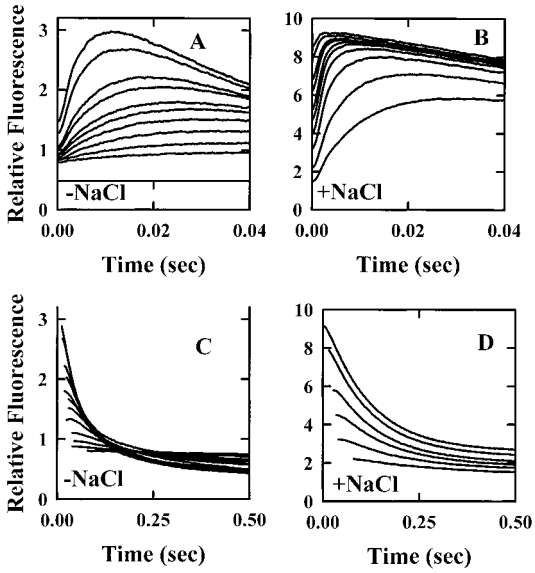

FIGURE 2: Fluorescence time courses for the reaction of enzyme with L-Ser (λ_{ex} = 420 nm). Panels A and B show the formation of the $E(Aex_1)$ species in the absence and the presence of 100 mM NaCl, respectively. Panels C and D show the decay of this species. Concentrations: $[\alpha_2\beta_2]$ = 10 μM, [L-Ser] = 0.125−60 mM (see Figure 3).

Figure 2 shows the concentration dependence of the time courses in stage I with isotopically normal L-Ser in the

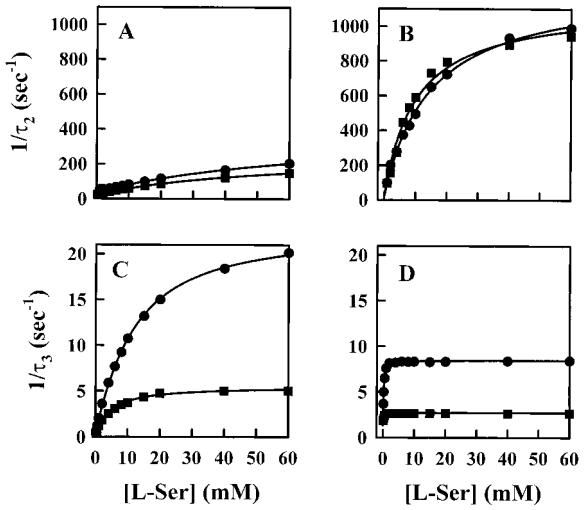

FIGURE 3: Dependencies of relaxation rate constants on the concentration of L-Ser for the reaction of $\alpha_2\beta_2$ with L-Ser in the absence (A, C) and presence (B, D) of 100 mM Na^+. Formation and decay of $E(Aex_1)$ were followed using the fluorescence signal of that species (λ_{ex} = 420 nm). In panels A and B, the relaxation rate constant ($1/\tau_2$) for the formation of $E(Aex_1)$ is shown as a function of [L-Ser]; in panels C and D, the concentration dependence of the relaxation rate constant ($1/\tau_3$) for the decay of $E(Aex_1)$ is shown. Symbols: circles, isotopically normal L-Ser; squares, [α-^{2}H]-L-Ser. Concentrations: [$\alpha_2\beta_2$] = 10 μM, [L-Ser] or [[α-^{2}H]-L-Ser] = 0.125−60 mM.

absence (A and C) and presence (B and D) of NaCl at shorter and longer time scales. The same analysis was carried out with the deuterated substrate (data not shown). Figure 3 shows both the dependence of the relaxation rate constant for the formation of the $E(Aex_1)$ species ($1/\tau_2$) on the L-Ser concentration in the absence and presence of NaCl (A, B) and the dependence of the first relaxation rate constant for the decay to the E(A-A) species ($1/\tau_3$) on the L-Ser concentration, also in the absence and presence of NaCl (C, D). The circles refer to isotopically normal L-Ser and the squares to [α-^{2}H]-L-Ser. The rate parameters presented in Figure 3 were derived from fitting the time courses shown in Figure 2 to sums of exponentials (eq 1).

The kinetic titration curves shown in Figure 3 were fit to the simplified three-step mechanism for stage I shown in eq 2

$$E + \text{L-Ser} \underset{k_{-1}}{\overset{k_1}{\rightleftharpoons}} E(\text{L-Ser}) \underset{k_{-2}}{\overset{k_2}{\rightleftharpoons}} E(Aex_1) \underset{k_{-3}}{\overset{k_3}{\rightleftharpoons}} E(\text{A-A}) \quad (2)$$

(see Discussion section). According to this mechanism, in a first, very rapid step $\alpha_2\beta_2$ forms an enzyme−substrate complex with L-Ser, E(L-Ser), which then decays to $E(Aex_1)$ and E(A-A). Because there is no detectable transient accumulation of either the *gem*-diamine species, $E(GD_1)$, or the L-Ser quinonoid species, $E(Q_1)$, these species were not included in this simplified mechanism. The data were analyzed within the framework of relaxation kinetic theory for the system of three equilibrating steps (eq 2) according to Bernasconi (*40*) with the further assumption that the first step equilibrates much faster than the second and third steps, i.e.

$$k_1\,[\text{L-Ser}] + k_{-1} \gg k_2, k_{-2}, k_3, k_{-3} \quad (3)$$

This assumption is in agreement with the time courses for $E(Aex_1)$ formation and decay. The dependence of the relaxations on the concentration of L-Ser is then described by

$$\frac{1}{\tau_2} = \frac{1}{2}(a+b) + \sqrt{[{}^1/_2(a+b)]^2 - k_3 b - a k_{-3}} \quad (4)$$

and

$$\frac{1}{\tau_3} = \frac{1}{2}(a+b) - \sqrt{[{}^1/_2(a+b)]^2 - k_3 b - a k_{-3}} \quad (5)$$

where

$$a = \frac{k_2 K_1[\text{L-Ser}]}{1 + K_1[\text{L-Ser}]} + k_{-2} + k_3;$$

$$b = \frac{k_2 K_1[\text{L-Ser}]}{1 + K_1[\text{L-Ser}]} - k_{-3}$$

Combining expressions, a set of four equations (eqs 6−9) can be defined that allows for the graphic evaluation of the rate and equilibrium parameters:

$$\frac{1}{\tau_2\tau_3} = k_2(k_3 + k_{-3})\frac{K_1[\text{L-Ser}]}{1 + K_1[\text{L-Ser}]} + k_{-2}k_{-3} \quad (6)$$

$$\frac{1}{\tau_2\tau_3 - (k_{-2}k_{-3})} = \frac{1}{k_2 K_1(k_3 + k_{-3})}\frac{1}{[\text{L-Ser}]} + \frac{1}{k_2(k_3 + k_{-3})} \quad (7)$$

$$\frac{1}{\tau_2} + \frac{1}{\tau_3} = k_2\frac{K_1[\text{L-Ser}]}{1 + K_1[\text{L-Ser}]} + k_{-2} + k_3 + k_{-3} \quad (8)$$

$$\frac{1}{(\tau_2^{-1} + \tau_3^{-1})(k_{-2} + k_3 + k_{-3})} = \frac{1}{k_2 K_1}\frac{1}{[\text{L-Ser}]} + \frac{1}{k_2} \quad (9)$$

The estimates of K_1, k_1, k_{-1}, k_2, k_{-2}, k_3, and k_{-3} obtained from this treatment were then used to fit the curves to the original equations, and the results are summarized in Table 1. These data show that in stage I K_1, k_2, k_3, and k_{-3} are strongly influenced by the binding of Na^+ and, as previously demonstrated by Lane and Kirschner (*39*) and by Drewe and Dunn (*33*), k_3 is subject to a large primary KIE. Table 2 shows the apparent dissociation constants for the formation of the $E(Aex_1)$ and E(A-A) species. The presence of Na^+ changes the apparent association constant for E(A-A) formation by ∼3-fold.

Similar results were obtained when the analogous analysis was carried out for stage I in the presence of IGP (Table 1). These data are in agreement with the finding that the cleavage of IGP at the α-site is slow with respect to stage I, and therefore, stage I of the β-reaction reaches a quasi-equilibrium before any significant amount of IGP has been cleaved (*17*, *20*, *41*, *42*). Because the titration curves used in this analysis are qualitatively very similar to those presented in Figure 3, these data are not shown.

Dependence of the First Half-Reaction on NaCl. Figure 4 shows the dependence of the fluorescence intensity due to $E(Aex_1)$ formation at equilibrium and the relaxation rate constants for the formation and the decay of $E(Aex_1)$ in stage

Table 1: Influence of NaCl and IGP on the Kinetic Parameters and Isotope Effects for Stage I of the β-Reaction[a,b]

substrates and MVC effectors	K_1 (mM^{-1})	EIE, K_1	k_2 (s^{-1})	KIE, k_2	k_{-2} (s^{-1})	KIE, k_{-2}	k_3 (s^{-1})	KIE, k_3	k_{-3} (s^{-1})	KIE, k_{-3}
L-Ser	0.014	0.7	370	1.54	25	1.25	23.0	3.96	0.7	3.5
[α-^{2}H]-L-Ser	0.020		240		20		5.8		0.2	
L-Ser, NaCl	0.070	0.78	1230	1.10	15	1.0	6.5	5.91	2.0	1.25
[α-^{2}H]-L-Ser, NaCl	0.090		1116		15		1.1		1.6	
L-Ser, IGP	0.020	1.0	540	1.52	23	1.04	40.5	2.53	4.9	0.75
[α-^{2}H]-L-Ser, IGP	0.020		354		22		16.0		6.5	
L-Ser, IGP, NaCl	0.070	1.0	1390	1.02	23	1.04	16.7	2.98	5.5	1.17
[α-^{2}H]-L-Ser, IGP, NaCl	0.070		1360		22		5.6		4.7	

[a] The kinetic parameters were obtained from the fitting of data such as those presented in Figures 2 and 3 to eqs 2−4 (see text). [b] Error limits for rate and equilibrium parameters are estimated to be as follows: K_1, ±10%; k_2, ±15%; k_{-2}, ±15%; k_3, ±5%; k_{-3}, ±15%. The combination of a larger amplitude and slower rate for the relaxation dominated by k_3 gives rise to a smaller percent error for k_3.

Table 2: NaCl and IGP Effects on Stage I of the β-Reaction: Apparent Dissociation Constants for the Formation of the E(Aex_1) and E(A-A) Species[a,b]

MVC and α-subunit effector/substrate	$K_d^{E(Aex1)}$ (mM)	$K_d^{E(A-A)}$ (mM)
−NaCl, −IGP	4.83	0.15
+NaCl, −IGP	0.17	0.05
−NaCl, +IGP	2.13	0.26
+NaCl, +IGP	0.24	0.08

[a] Reactions of $\alpha_2\beta_2$ with L-Ser in the absence and in the presence of NaCl and/or IGP were carried out as described in the legends to Figures 2 and 3. [b] Values of $K_d^{E(Aex1)} = [\alpha_2\beta_2][\text{L-Ser}]/[E(Aex_1)]$ and $K_d^{E(A-A)} = [\alpha_2\beta_2][\text{L-Ser}]/[E(A\text{-}A)]$ are calculated using parameters given in Table 1.

I on the concentration of Na^+. The time courses were measured by observing the fluorescence of E(Aex_1). MVC-free enzyme was mixed with 60 mM L-Ser with varying amounts of NaCl present. The relaxation rate constants were determined and plotted as a function of NaCl concentration (panels B and C). Panel A of Figure 5 shows the fluorescence due to the E(Aex_1) species at equilibrium as a function of [NaCl] after reaction. The formation of E(Aex_1) in the presence of NaCl is biphasic; the faster phase depends on [NaCl] while the slower phase is independent of [NaCl] (relaxation rate ~100 s^1). The contribution to the total (increasing) amplitude from this relaxation decreases with increasing [NaCl]. The dependence of the faster phase (τ_2) on [NaCl] is shown in panel B. The decay of E(Aex_1) is biphasic; the faster decay phase (τ_3) is dependent on [NaCl] and shows a decrease in the relaxation rate constant ($1/\tau_3$) with increasing [NaCl] (panel C).

The behavior of the preequilibrated mixture of E(Aex_1) and E(A-A) after the addition of MVCs was investigated by rapidly mixing $\alpha_2\beta_2$ and L-Ser with Na ions (Figure 5). After the MVC-free system was mixed with Na^+, a redistribution in favor of E(Aex_1) occurs. At concentrations of NaCl varying from 125 μM to 10 mM, the rate of redistribution was measured by following the increase in fluorescence intensity due to E(Aex_1) formation (Figure 5A). These time courses show that the formation of E(Aex_1) is a monophasic process and that the relaxation rates decrease with increasing metal ion concentration. In panel B, the relaxation rate constant for the process is shown as a function of NaCl concentration. The value of the *y*-intercept of this plot is about 7−10 s^{-1}, and the curve approaches a limiting value of ~1.9 s^{-1} for high concentrations of NaCl. The decrease in the relaxation rate constant with increasing concentration of NaCl suggests a mechanism involving a slow step

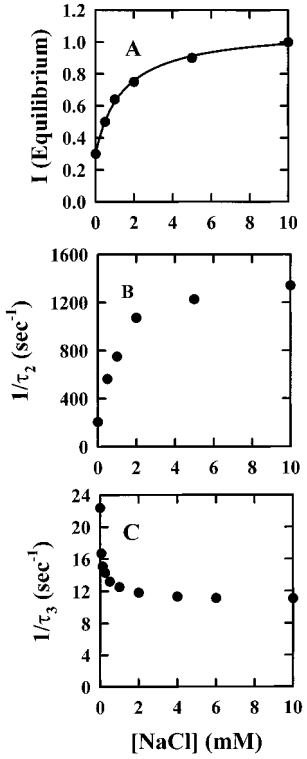

FIGURE 4: Influence of Na^+ concentration on the interconversion of E(Aex_1) and E(A-A). Panel A shows the dependence of the equilibrium fluorescence intensity of E(Aex_1) with respect to [NaCl]. Panels B and C show respectively the concentration dependencies on [NaCl] of the rate of formation ($1/\tau_2$) and decay ($1/\tau_3$) of E(Aex_1). Concentrations: $[\alpha_2\beta_2] = 15\ \mu M$; [L-Ser] = 60 mM at pH 7.8. The ionic strength was kept constant with tetramethylammonium chloride.

preceding the binding of Na^+ (see Discussion). A mechanism of that type can be fit with the equation:

$$1/\tau_2 = k_1 + \frac{k_{-1}}{1 + K_2[Na^+]} \qquad (10)$$

where k_1 is the forward rate constant of a unimolecular reaction (conformational change), k_{-1} is the reverse rate constant of that step, and $K_2 = k_2/k_{-2}$ is the association constant for Na^+ binding for the scheme:

$$A \underset{k_{-1}}{\overset{k_1}{\rightleftharpoons}} B \underset{k_{-2}}{\overset{k_2, Na^+}{\rightleftharpoons}} B(Na^+) \qquad (11)$$

Kinetic Isotope Effects on Individual Steps of Stage I of the β-Reaction. In stage I, the formation of E(A-A) from

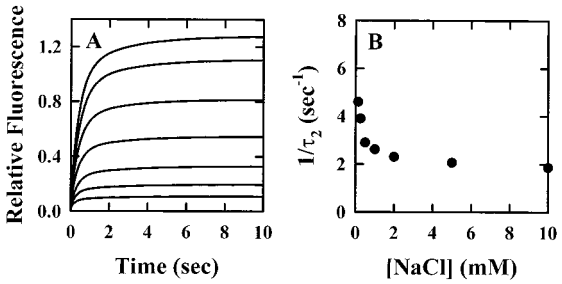

FIGURE 5: Relaxation of the equilibrium mixture of E(Aex$_1$) and E(A-A) after reaction of a preequilibrated mixture of enzyme and L-Ser with NaCl. Panel A displays the fluorescence time courses for the relaxation. The redistribution favors the E(Aex$_1$) species at the different NaCl concentrations. In panel B the relaxation rate constant ($1/\tau_2$) for this process is shown as a function of [NaCl]. Concentrations in (A) and (B) were as follows: [$\alpha_2\beta_2$] = 36 μM; [L-Ser] = 40 mM; [NaCl] = 0.125−10 mM.

E(Aex$_1$) involves the abstraction of the α-proton and is subject to a primary kinetic isotope effect (*33*, *39*, *43*). Single-wavelength, absorbance stopped-flow time courses were measured at 350 nm. The peak at 350 nm has been assigned to the E(A-A) spectrum (*33*) and, therefore, serves as a signal for the formation and decay of this species. The increase in absorbance at this wavelength is biphasic; however, the slower phase shows a very small amplitude and, in the presence of NaCl or NH_4Cl, is negligible. The KIE on the faster phase was examined using isotopically normal D,L-Ser and [α-^{2}H,β-$^2H_2$]-D,L-Ser in the absence of MVCs, in the presence of NH_4^+, or in the presence of Na^+. The KIEs on specific rate constants were also investigated in the fluorescence stopped-flow analysis shown earlier using [α-^{1}H]-L-Ser and [α-^{2}H]-L-Ser (see Figure 2 and Table 1).

The data in Table 1 compare the KIEs for the specific rate constants (defined by eqs 2−4) extracted from the detailed relaxation kinetic analysis. This analysis shows that, in the absence of MVCs, the KIE on k_3 is 4.0 ± 0.4, while in the presence of Na^+, a value of 5.9 ± 0.5 is obtained. Reaction in the reverse direction shows a KIE on k_{-3} of 3.5 ± 0.3 in the absence of MVCs and 1.25 ± 0.15 in the presence of Na^+. The very large equilibrium isotope effect predicted by these results (∼4.7 in the presence of Na^+) is consistent with the formation of a low-barrier H-bond (LBHB) as E(Aex$_1$) is converted to E(A-A), a finding consistent with previous evidence for an LBHB in this step (*44*).

Table 3 summarizes the relaxation rate constants and the observed isotope effects determined in the reactions of isotopically normal D,L-Ser and [α-^{2}H,β-$^2H_2$]-D,L-Ser with E(Ain). An apparent primary kinetic isotope effect is detected for the faster phase, both in the absence and in the presence of MVCs. The effect is slightly larger in the presence of NH_4Cl (3.0 ± 0.3 versus 2.2 ± 0.2 without MVCs or with NaCl). The fact that the E(Aex$_1$) species does not accumulate transiently to the same degree in the absence of MVCs as in the presence of Na^+ does not eliminate the kinetic isotope effect. This finding demonstrates that the formation of the E(A-A) species is kinetically limited by the decay of the E(Aex$_1$) species both in the absence and in the presence of MVCs and excludes the possibility that a conformational change limits the rate of E(A-A) formation.

Isotope Effects on Enzyme Activity in the Steady State. Steady-state activity measurements for the β-reaction were performed to investigate the effects of MVCs on the rate-limiting character of individual steps. Studies were carried out using isotopically normal L-Ser and [α-^{2}H]-L-Ser. The results of these experiments are summarized in Table 4. These data show that, in the absence of MVCs, substitution of ^{1}H by ^{2}H at the α-C of L-Ser has essentially no effect on the turnover rates of either the β-reaction or the $\alpha\beta$-reaction. When examined in the presence of either Na^+ or K^+, the activity of the β-reaction shows large, observed, primary KIEs of 5.3 ± 0.5 and 3.0 ± 0.3, respectively. Surprisingly, this same experiment carried out in the presence of NH_4^+ showed no primary KIE.

Ammonium Ion Effects on the Distribution of Intermediates: A Static UV/Visible Absorbance Analysis. Figure 6 shows the equilibrium spectra obtained after reaction of $\alpha_2\beta_2$

Table 3: Influence of MVCs on Relaxation Rate Constants and Deuterium Isotope Effects for the Formation of the E(A-A) Species in Stage I of the β-Reaction[a,b]

reactants	$1/\tau_1$ (s^{-1})	KIE (H/D)	$1/\tau_2$ (s^{-1})	KIE (H/D)
D,L-Ser, no MVCs	18.8			
[α-^{2}H,β-$^2H_2$]-D,L-Ser, no MVCs	8.4	2.2	1.5	1.6
D,L-Ser, NaCl	9.1			
[α-^{2}H,β-$^2H_2$]-D,L-Ser, NaCl	4.1	2.2		
D,L-Ser, NH_4Cl	68			
[α-^{2}H,β-$^2H_2$]-D,L-Ser, NH_4Cl	23	3.0		

[a] $\alpha_2\beta_2$ was reacted with isotopically normal and ^{2}H-substituted serines both in the absence and in the presence of 100 mM NaCl or 50 mM NH_4Cl. Relaxation rate constants were determined from single-wavelength time courses measured at 350 nm. [b] The error limits on relaxation rates and KIEs were estimated to be as follows: $1/\tau_1$, ±10%; $1/\tau_2$, ±15%; KIEs, ±<5%.

Table 4: Influence of MVCs and Effectors on Primary Kinetic Isotope Effects and on the Activity of the β-Reaction[a,b]

isotope	MVC effector	$v_i/[E_0]$ (s^{-1})	isotope effect (H/D)
L-Ser	none	2.0	
[α-^{2}H]-L-Ser	none	1.8	1.28
L-Ser	NaCl	8.0	
[α-^{2}H[-L-Ser	NaCl	1.5	5.3
L-Ser	KCl	12	
[α-^{2}H]-L-Ser	KCl	4	3.0
L-Ser	NH_4Cl	10.3	
[α-^{2}H]-L-Ser	NH_4Cl	7.9	1.3

[a] Steady-state rate measurements were measured under the following conditions: [$\alpha_2\beta_2$] = 0.4 μM; [serine derivative] = 40 mM; when present [NaCl] = 100 mM, [KCl] = 100 mM, or [NH_4Cl] = 50 mM. [b] Error limits were estimated to be as follows: activity, ±10%; KIEs, ±<5%.

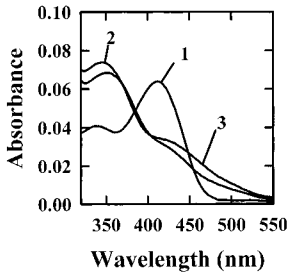

FIGURE 6: UV/vis static absorbance spectra for 5 μM $\alpha_2\beta_2$ measured under the following conditions: enzyme alone (1); reaction with 40 mM L-Ser (2); reaction with 40 mM L-Ser and 50 mM NH_4Cl (3).

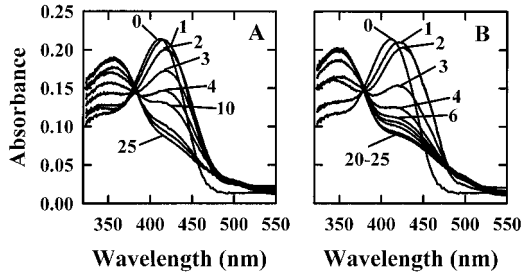

FIGURE 7: RSSF spectra for the reaction of $\alpha_2\beta_2$ with L-Ser in the absence of NH_4Cl (panel A) and in the presence of NH_4Cl (panel B). Concentrations: $[\alpha_2\beta_2] = 10\ \mu M$; [L-Ser] = 40 mM; $[NH_4Cl]$ = 50 mM where present. Timing sequence 2 was used (see Materials and Methods).

with L-Ser. In agreement with Woehl and Dunn (*2*), in the absence of an MVC, E(Ain) (spectrum 1) is converted to an equilibrating mixture of $E(Aex_1)$ and E(A-A) (spectrum 2) that is dominated by E(A-A). Although the equilibrium still favors the E(A-A) species in the presence of NH_4^+ (spectrum 3), there is a slightly larger proportion of $E(Aex_1)$ present. Hence, NH_4^+ stabilizes the external aldimine, however, not to the same extent as does K^+ or Na^+ (*2*).

Single-Wavelength Stopped-Flow Titration. The NH_4^+ concentration dependence of the maximum transient amplitude of the transient quinonoidal absorbance in the reaction of the E(A-A) species with indole was used to obtain an apparent dissociation constant for NH_4^+ binding. The apparent dissociation constant of 0.45 mM for NH_4^+ indicates that this ion binds more tightly than either Na^+ or K^+ (apparent values of 1.5 and 5 mM, respectively).

Rapid-Scanning Stopped-Flow (RSSF) Measurements. RSSF measurements were performed to investigate the influence of NH_4^+ on the transient accumulation of intermediates. Figure 7 shows the reaction of $\alpha_2\beta_2$ with L-Ser in the absence (panel A) and in the presence (panel B) of 50 mM NH_4Cl. These time-resolved spectra clearly show that, while the E(A-A) species accumulates to about the same degree at equilibrium after reaction of $\alpha_2\beta_2$ with L-Ser, the $E(Aex_1)$ species accumulates to a higher degree in the transient phase in the presence of NH_4Cl. The second spectrum obtained after mixing (at about 16 ms) in the absence of NH_4Cl exhibits a λ_{max} similar to that of the enzyme alone, suggesting that the envelope of bands is dominated by the spectrum of E(Ain); however, in the presence of NH_4Cl, even the first spectrum after mixing (at ~8 ms) shows the λ_{max} of the $E(Aex_1)$ species.

DISCUSSION

The mechanism of action of MVCs in modulating protein function is a neglected area of research that consequently has lagged behind many other areas of cofactor investigation. More than 100 enzymes are known to be activated by MVCs (*1*, *45*−*47*), including such diverse enzymes as pyruvate kinase (*48*), tryptophan synthase (*2*, *3*), thrombin (*49*), GroEL (*50*), and dialkylamino acid decarboxylase (*51*). Nevertheless, current biochemistry textbooks generally acknowledge only those biological functions for Na^+ and K^+ associated with membrane potential, nerve signal transmission, and the Na^+ and K^+ pumps. One reason for this neglect has been the lack of three-dimensional structural information concerning the binding sites for Na^+, K^+, and NH_4^+ in proteins. The similarities in the X-ray scattering factors of these ions to those of water and hydronium ion (10 electrons) have made identification of MVC sites difficult. It is only in the past four years that MVC sites have been described in enzyme structures (see ref *1*). The available structures show that, in all but one case, the MVC site is located >6 Å distant from the catalytic site, indicating that these ions should be classified as cofactors that act through binding interactions broadly defined as allosteric ("other site") which modulate the conformation of the protein (*1*).

Structural Elements Identified by X-ray Crystallography, Site-Directed Mutagenesis, and Solution Studies. Several structures of tryptophan synthase have been solved (*4*, *5*, *12*). These include (a) the native $\alpha_2\beta_2$ bienzyme complex (*12*), (b) the complex with IPP bound to the α-site (*12*), (c) the Na^+, K^+, and Cs^+ forms of $\alpha_2\beta_2$ (*4*), (d) the L-Ser and L-Trp external aldimine forms of the βK87T mutant and the influence of IPP or GP on the structures of these intermediates (*5*), and (e) the structure of the αD60N mutant with IGP bound to the α-site (*52*) and the structure of the E(A-A) complex with 5-fluoro-IGP bound to the α-site (*53*). Comparisons among these structures reveal a wealth of information which appears relevant to the conformational transitions which have been identified via solution studies involving ligand binding to the α-site, MVC binding to the MVC sites, and covalent reactions at the β-site (*6*). Taken together, these structural determinations and solution studies show that the α-site of $\alpha_2\beta_2$ has an open conformation wherein loops 2 and 6 are highly disordered in the crystal structure (*5*, *12*). This structure shows that the entrance to the β-site is via a narrow opening located close to the β−β subunit interface (Figure 8B). When the β-site of the βK87T mutant is in the form of either the L-Ser or L-Trp external aldimines, binding of IPP or GP to the α-subunit gives a crystal structure where loop 6 is folded down onto loop 2 over the α-site to give a closed conformation (*5*) (Figure 8A). Examination of the conformation of the β-subunit in this complex shows that, due to a rotation of one β-subunit domain relative to the other, the narrow opening present in the unliganded protein has become closed (Figure 8C).[2]

The structural studies of the MVC-substituted tryptophan synthases show the presence of two MVC sites. One site located about 8 Å from the β-site binds Na^+, K^+, or Cs^+ (the Na^+/K^+ site, Figure 9). A second site located at the β−β interface on the 2-fold symmetry axis binds a second Cs^+

[2] The experiments of Brzovic et al. (*20*) and Leja et al. (*24*) have established that the conversion of $E(Aex_1)$ to E(A-A) is the allosteric trigger which activates the α-site, while conversion of $E(Q_3)$ to $E(Aex_2)$ triggers conversion of the α-site back to the low-activity state. These changes are accompanied by the interconversion of the conformations of $\alpha\beta$ dimeric units between open and closed conformations (*6*, *16*, *25*). Therefore, the finding that the $E(Aex_1)$ complexes of the βK87T mutant with GP or IPP give conformations where the α- and β-sites appear to be closed requires comment. In our view, either these structures represent the partially closed, low-activity, conformations postulated by Pan et al. (*25*) for the external aldimine complexes, or the mutation of βLys167 to Thr switches these complexes to the closed conformation. However, the α-sites of these complexes are not activated. Schneider et al. (*51*) report that there are significant differences between the conformation of the complex of E(A-A) with 5-fluoro-IGP and the conformations of the $E(Aex_1)$ complexes with GP and IPP involving residues which form part of the network of protein residues through which allosteric interactions seem to be communicated. Consequently, the closed structures obtained with the $E(Aex_1)$ complexes of GP and IPP are more likely to represent the partially closed structure.

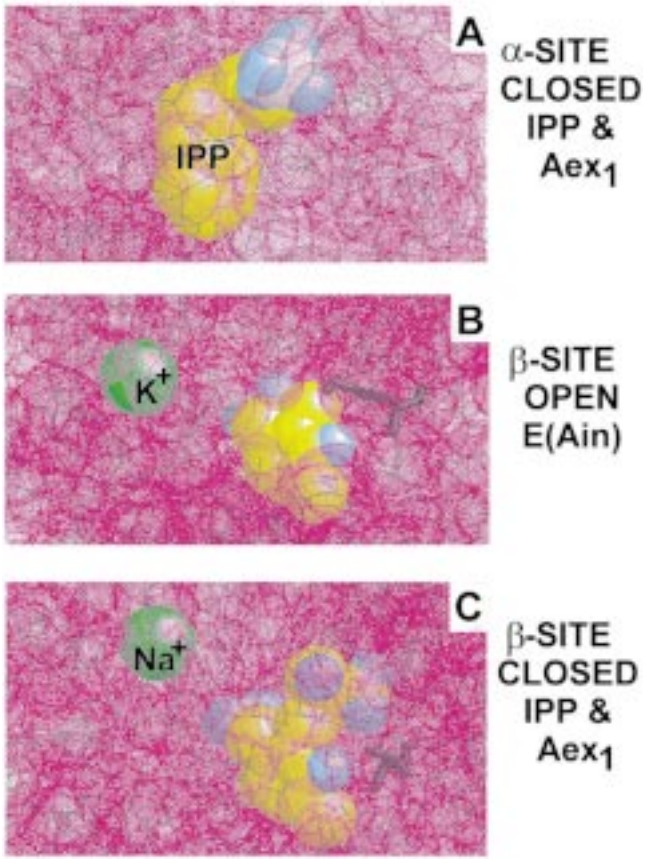

FIGURE 8: X-ray structure diagrams of tryptophan synthase showing the van der Waals surfaces of the protein, the monovalent cation cofactor, and ligands in the vacinity of the α- and β-sites for closed (A, C) and open (B) conformations. The van der Waals surfaces of the protein are shown as a magenta dot surface, PLP, PLP derivatives, IPP, Na^+, and K^+ are all shown as space-filling models, and residue β87 (Lys in panel B and the mutation to Thr in panel C) is shown as a black stick model. Color scheme: ligand C and N, yellow; ligand O, blue; ligand P, white; protein van der Waals dot surface, magenta; protein wire frame, black; K^+ or Na^+, green; β87, black. (A) The "closed" structure of the α-site viewed from the solvent looking into the site. In this complex, loops 2 and 6 of the α-subunit are closed down over the substrate analogue, IPP, blocking off the site to access from the solvent. The β-site is in the form of the L-Ser external aldimine (viz., C). Coordinates were taken from 2TRS.PDB (*5*). (B) The "open" or "partially closed" structure of the β-site of E(Ain) viewed from the solvent. The van der Waals surfaces show a clear path from solvent down to C3, O3, and C4′ of the PLP cofactor and to the ε-N of βK87. Coordinates were taken from 1TTQ.PDB (*4*). (C) The "closed" structure of the β-site occupied by the L-Ser external aldimine of the βK87T mutant enzyme viewed from the same orientation as in (B). IPP is bound to the α-site in this structure (viz., A). Coordinates were taken from 2TRS.PDB (*5*). In this complex, access from solvent into the β-site is almost completely closed off by the van der Waals surface of the protein, indicating that β-subunit domain movements have closed the β-site. These drawings were created using RasMol 2.

(the Cs^+ site) (*4*). The ligands to the Na^+/K^+ site consist of a set of three carbonyl oxygens comprised of the backbone carbonyls of Phe306, Ser308, and Gly232 plus two water molecules in the Na^+ complex and one in the K^+ complex (Figures 9 and 10). When bound to this site, Cs^+ recruits three additional carbonyls (Val231, Gly268, and Leu304) but excludes the waters. In the Na^+ structure, βD305 takes up two orientations, one where βK167 forms a salt bridge to βD305 (Figures 9A and 10) and one where the side chain of βD305 is rotated away (not shown). In the K^+ and Cs^+ structures, the position of the side chain of βK167 flips ~180° and forms a new salt bridge across the α−β subunit interface to αD56 (Figures 9B and 10). This rearrangement is accompanied by an increase in the disorder of the βD305 side chain, and the side chains of βF280 and βY279 move from a conformation where the tunnel is partially blocked in the Na^+ structure to a conformation where these residues form part of the tunnel lining. The external aldimine structures of the βK87T mutant with Na^+ bound to the Na^+/K^+ site and IPP or GP bound to the α-site give a conformation where βK167 forms the salt bridge to αD56 (*5*). In the L-Ser external aldimine structure in the absence of IPP or GP, the side chain of βD305 forms an H-bond to the L-Ser hydroxyl. In the IPP and GP complexes, the βD305 carboxylate is rotated away. The substrate/product side chains of the L-Ser and L-Trp external aldimines have different conformations; the L-Ser hydroxyl of $E(Aex_1)$ is tilted forward so that an H-bond is formed with βD305, while the indole ring of $E(Aex_2)$ is tilted back into the site so that the ring NH forms an H-bond to βE109. In the E(A-A) complex with 5-fluoro-IGP, the position of the carboxylate of βD305 is similar to that found in the $E(Aex_1)$ and $E(Aex_2)$ structures and points away from the coenzyme.

Solution Evidence for Functional Conformational Transitions in Tryptophan Synthase Catalysis. The above-described structures imply that, in solution, E(Ain) has an open structure, while the L-Ser and L-Trp external aldimine complexes with IPP or GP and the E(A-A) complex have more closed structures wherein loop 6 is closed down over the α-site onto loop 2. In these closed structures, with either Na^+ or K^+ bound to the Na^+/K^+ site, βK167 forms a salt bridge across the α−β interface to αD56 (Figures 1 and 10). The rapid kinetic studies of Dunn et al. (*16*) and Brzovic et al. (*41*, *54*) established that when the β-site is in the form of the E(A-A) complex with GP or G3P bound to the α-site, the αβ-dimeric unit of the bienzyme complex assumes a closed conformation which prevents the escape of indole into solution from the β-site (*15*, *16*, *24*) (Figure 1B). Mutations of key residues within loop 2 or 6 of the α-subunit were found to prevent formation of the closed structure of the α-subunit, thus making the β-site freely accessible, presumably via the α-site and the tunnel (*41*, *53*). Solution kinetic studies have established that (in the absence of IPP or GP) E(Ain), $E(Aex_1)$, and $E(Aex_2)$ are forms of the enzyme where the α-site resides in a low-activity state (*17*, *19*, *20*, *24*, *25*). In this regard it is noteworthy that, in the $E(Aex_1)$(IPP) complex, αE49, the residue believed to be the acid−base catalyst which protonates the C-3 of indole and removes the 3′-hydroxyl proton of IPP during C−C bond scission, is located 6 Å distant from IPP and is folded away from the scissile bond. In the GP complex, it is 4.8 Å away, still too far to participate in catalysis (*5*). A recent report (*52*) shows that this residue rotates to a position suitable for catalysis in the complex of the αD60N mutant complex with IGP. However, this complex appears to retain the open conformation, and therefore its relevance to catalysis is unclear. The E(A-A) complex with 5-fluoro-IGP shows that formation of this species from the E(Ain)(5-fluoro-IGP) complex results in a conformational transition involving a rigid body movement of a subdomain of the β-subunit which causes changes in loop 2 of the α-subunit (*53*), but the chemical origins of the activation of the α-site apparently remain obscure.

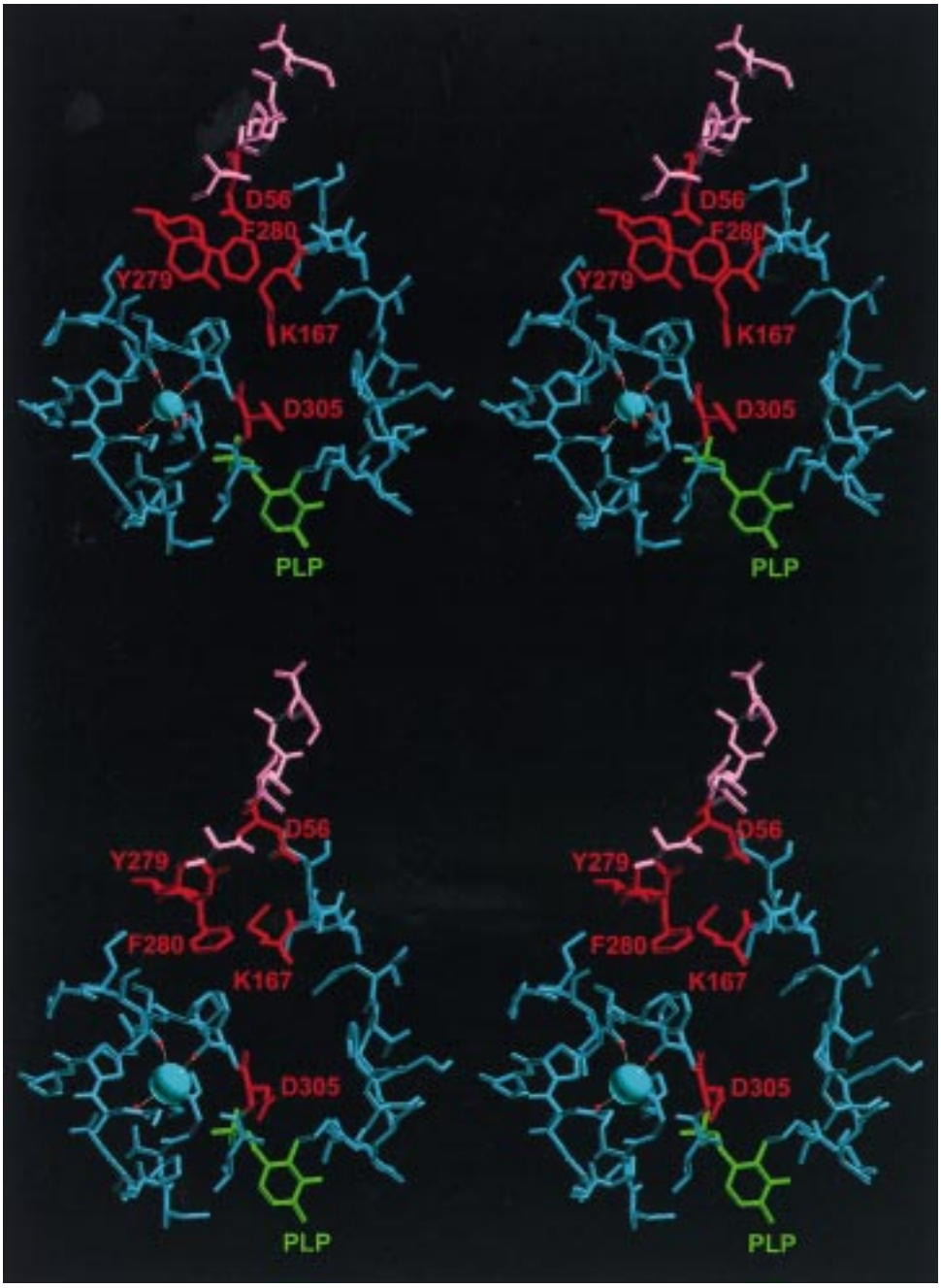

FIGURE 9: Stereo diagrams for E(Ain) showing the structures of the metal site and the βK167−βD305 salt bridge (A) (Na^+ complex, upper set) and the βK167−αD56 salt bridge (B) (K^+ complex, lower set). Coloring scheme: blue, β-site residues; pink, α-site residues; green, PLP. Salt bridge residues and residues with conformations affected by substitutions at the MVC site (βK167, αD56, βD305, βF280, and βY273) are labeled in red. The carbonyl oxygens of the protein residues and water molecules making up the coordination spheres of the metal ions also are shown in red. The metal ions are scaled to their ionic radii (Na^+ = 1.02 Å, K^+ = 1.38 Å). The coordinates used to generate the set shown in (A) were provided by Sangkee Rhee for the Na^+ complex of E(Ain). The coordinates used in (B) were taken from the Brookhaven database file ITTQ.PDB (*4*).

Pan and Dunn (*25*) reported experiments with the fluorescent probe ANS showing that the conformation state of $\alpha_2\beta_2$ is dependent both on the covalent state of the β-subunit and on the ligation state of the α-subunit. On the basis of the affinity of the enzyme for ANS, three classes of conformational states were identified, an open conformation assigned to E(Ain) (Figure 1B), partially closed conformations of $\alpha\beta$-dimeric units assigned to E(Aex_1) and E(Aex_2), and closed conformations assigned to E(A-A) and E(Q) species (Figure 1B). These conformational classifications were found to correlate with the activity states of the α-site; the open and partially closed conformations were found to correspond to states with low α-site activity, while the closed conformation corresponds to the activated state of the α-site. In view of the recently published structures of the E(Aex_1) and E(Aex_2) complexes, it seems reasonable to assign these as the partially closed, low-activity conformations identified by Pan and Dunn (*25*), and the structure of the E(A-A) species (*53*) should correspond to the high-activity conformation.[2] A structure corresponding to the high-activity, completely closed structure predicted for the E(Q) species has not yet been determined.

Metal Ion Effects on Stage I. As demonstrated in Figure 3 and Table 1, MVC binding clearly influences kinetic

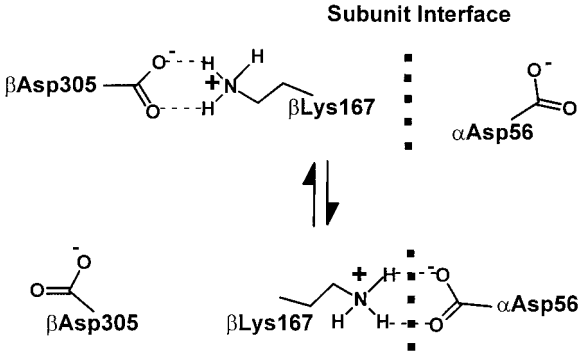

FIGURE 10: Cartoon showing the rearrangement of βK167 between the alternative salt bridge conformations involving βD305 or αD56. Dashed lines show the $\alpha\beta$-subunit interface.

parameters in the first half-reaction. In the absence of the metal ion, the E(Aex$_1$) species forms in a monophasic process with a relaxation rate that increases with increasing L-Ser concentration (Figure 3A). In the presence of the metal ion, two phases can be detected, one that increases in rate with increasing concentration of substrate ($1/\tau_2$) and one that is independent of substrate concentration with a relaxation rate of 50−100 s^{-1} ($1/\tau'_2$). The dependency on the serine concentration reveals changes in several rate parameters: the formation rate (k_2) for the E(Aex$_1$) species is stimulated by ∼3-fold in the presence of the metal ion (from 370 to 1230 s^{-1}), while the decay rate (k_3) to form E(A-A) is reduced by ∼3-fold, from 23 to 6.5 s^{-1} (Table 1). The formation of the enzyme−substrate complex is favored by an ∼4-fold change in the association constant (K_1). As can be seen in Figure 3 (panels C and D), those changes result in a saturation of E(A-A) formation at a significantly lower concentration of L-Ser, and the relaxation rates for E(A-A) formation ($1/\tau_3$) are noticeably higher in the presence of the metal ion.

Evidence That the Two Forms of E(A-A) Correspond to Open and Closed States of the β-Subunit. The dependencies of relaxation rates with respect to variation of the metal ion concentration shown in Figure 4, together with the data in Figures 2 and 3, are consistent with the conclusion that MVC binding changes the energy surface of the first half-reaction and yields an altered equilibrium of active and less active states of the E(A-A) species. The formation of the E(Aex$_1$) species shows an increase in the relaxation rate constant with increasing concentration of the metal ion. Again, however, a second slower and smaller amplitude increasing phase with a rate of ∼100 s^{-1} can be detected that is independent of metal ion concentration. The dependency of $1/\tau_2$ on the metal ion concentration follows a hyperbolic curve, reflecting metal ion binding to the enzyme at an earlier step in the pathway. The decay process ($1/\tau_3$) decreases gradually with increasing metal ion concentration. This decrease is caused by the decreased rate of formation of the less active state. Although a minimal linear mechanism was employed for the analysis of the kinetic behavior presented in Figures 2 and 3, the results obtained for the second half-reaction suggest that two forms of the E(A-A) species must be invoked (see ref *55*).

Schneider et al. (*53*) and McDowell et al. (*56*) have postulated that the α-aminoacrylate Schiff base, E(A-A), is in equilibrium with a methyl ketoimine tautomer, E(MK), and therefore one might propose that the two forms of E(A-A) inferred from the kinetic experiments reported in Figures

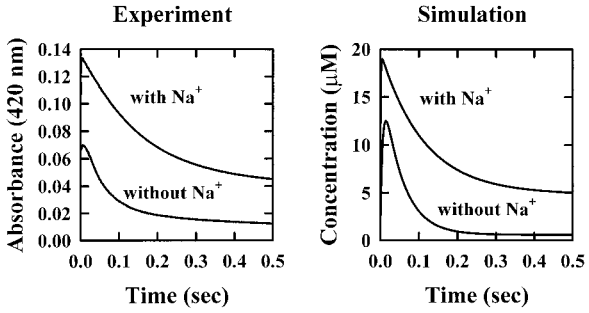

FIGURE 11: Comparison of experimental (A) and simulated (B) time courses for the formation and decay of E(Aex$_1$) in stage I, both in the presence of 100 mM Na^+ and in the absence of any MVCs. The experimental time courses show the formation and decay of the E(Aex$_1$) intermediate measured by the absorbance changes at 420 nm. Concentrations: 10 μM $\alpha_2\beta_2$ and 40 mM L-Ser. Simulations were performed as described under Materials and Methods.

2−5 actually correspond to the formation of E(A-A) and E(MK). However, we reject this explanation on the grounds that the postulation of the E(MK) intermediate is incompatible with the very large equilibrium isotope effect observed for the interconversion of E(Aex$_1$) and E(A-A) (*44*), and therefore an E(MK) species is unlikely to be in equilibrium with E(A-A). The energy barrier to rotation about the Cα−Cβ single bond in E(MK) should be very low, and therefore the presence of E(MK) would require that the true EIE for this equilibration be significantly larger than that predicted for the upper limit expected for a EIE due to low-barrier H-bonding.

Therefore, we postulate that the two states identified by the above experiments correspond to a closed β-subunit of high activity through which most of the reaction proceeds and an open β-subunit conformation of low activity. It has long been proposed that the E(A-A) species exists in two conformations (*11*, *20*, *25*, *39*). Taking into account the results of the following report (*55*) concerning the mechanism of stage II, our findings are consistent with a pathway in which E(Aex$_1$) reacts to form two conformations of the E(A-A) species. It then follows that the rate parameters described for the decay of the E(Aex$_1$) species represent the envelope of two parallel steps, postulated respectively to be formation of E(A-A)$_{closed}$ and formation of E(A-A)$_{open}$. Therefore, the kinetic parameters for E(A-A) formation are the sum of the kinetic parameters for the two branches. Simulation studies that take into account the experimental results for both stage I and stage II lead to a set of rate parameters that model the general behavior of both stages. Figure 11 compares the observed and simulated time courses for the formation and decay of E(Aex$_1$). The mechanism assumed for these simulation studies is shown in Figure 12. The MVC effects (Figures 3−6) suggest that the formation of the more active, closed, form is changed relatively little and shows a rate of formation for E(A-A)$_{closed}$ of about 4 s^{-1} with and without metal ion present. The formation of the less active, open, form is slowed considerably in the MVC-bound forms (from about 18 to about 3 s^{-1}). This analysis provides an explanation for the higher relaxation rate constant ($1/\tau_3$) observed in the absence of the metal ion for the appearance of the E(A-A) species.

The kinetic studies on the reaction of E(A-A) with Na^+ provide evidence indicating that the interconversion between

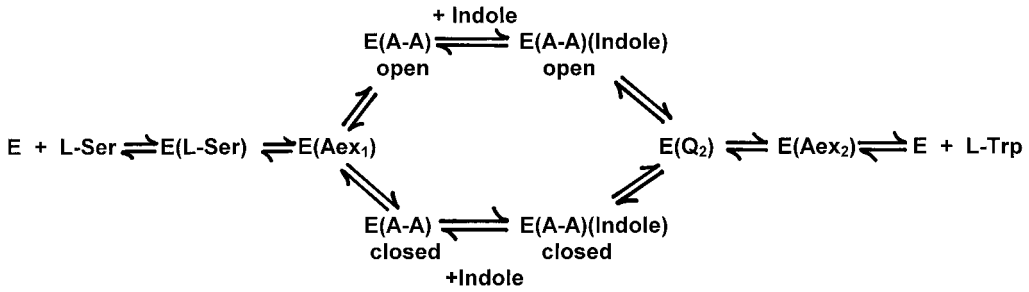

FIGURE 12: Mechanisms for stage I and stage II of the β-reaction.

the two conformations of E(A-A) is slow (see below). This happenstance is the reason why the branched nature of the pathway (i.e., existence of open and closed forms in parallel) can only be detected for that segment of the pathway involving the conversion of E(A-A) to E(Q_3). Although all of the different intermediates almost certainly exist in equilibrium between at least two conformations (*25*), for those steps where the rate of interconversion among states is very fast, the observed kinetic behavior will be indistinguishable from that of a single species.

In the reaction of the equilibrium mixture of $\alpha_2\beta_2$ and L-Ser with Na^+ ions, $1/\tau_{Na}$ for E(Aex_1) formation decreases with increasing [NaCl] from an extrapolated value for the *y*-intercept of around 7−9 s^{-1} to a value of about 2 s^{-1} at high concentrations of NaCl (Figure 5B). According to the mechanism shown in Figure 12, the kinetic analysis of the L-Ser reaction yields a rate constant of 6.5 s^{-1} for E(A-A) formation and a value of about 2 s^{-1} for the rate constant of the reverse reaction. Then, assuming fast binding of the metal ion to E(A-A), the expression for the relaxation rate constant of E(Aex_1) formation is

$$\frac{1}{\tau_{Na}} = k_{Na}\frac{K_1[Na^+]}{1 + K_1[Na^+]} + k_{-Na} \qquad (12)$$

The value for k_{Na} in this expression is identical with k_{-3} from Table 1, and k_{-Na} is identical with k_3 from Table 1. The expected relaxation rate constant should therefore *increase* with the metal ion concentration from about 6.5 to 8.5 s^{-1}. However, the observed rate *decreases* with increasing metal ion concentration, and the final value is 5−6-fold slower than the expected value for this mechanism. One possible interpretation of this result is that a conformational change must take place prior to metal ion binding. Such a mechanism would account for the observed decrease in relaxation rate constant with increasing ligand concentration. Since the binding constants of the different conformations of E(A-A) for the metal ion are not known, and since we only have rough estimates both for the equilibrium between active and inactive conformations and for the forward and reverse rates for formation of the two E(A-A) conformations, the model cannot be quantitatively validated. However, there is no evidence that the E(Aex_1) species interconverts slowly between open and closed states. The first intermediate on the pathway to demonstrate behavior in agreement with a slow interconversion is the E(A-A) species. It is, therefore, very likely that the active conformation of the E(A-A) species binds the metal ion rapidly; however, the less active form, which predominates in the absence of the metal ion, shows very little affinity for the metal ion and must first undergo the conformational change to the more active state in order to bind the metal ion. The E(Aex_1) species is then formed from MVC-bound E(A-A).

MVC Effects on Bond Scission. Kinetic isotope effects (KIEs) were determined both for the individual steps of stage I and for the overall activity in the β-reaction (Figure 2 and Tables 3 and 4). In stage I, the breaking of the bond to the α-proton of E(Aex_1) results in a primary KIE on the disappearance of that species (*33*, *39*, *44*, *55*). Single-wavelength stopped-flow measurements showed the expected isotope effects on $1/\tau_3$ of stage I (Figure 2): i.e., a primary KIE is detected on E(A-A) formation both in the absence and in the presence of MVCs. When subjected to detailed analysis via relaxation kinetic theory (Table 1), the KIE on the specific rate constant for the C−H bond scission step in the absence of MVCs is 4.0 ± 0.4. In the Na^+-activated form of the enzyme, this KIE is increased to a value of 5.9 ± 0.5, indicating that the nature of the transition state for this step is altered by the allosteric effects of Na^+ binding. The magnitudes of the KIEs on the reverse steps indicate that, in the absence of MVCs, the KIE for interconversion of E(Aex_1) and E(A-A) appears normal (∼1.1), whereas in the presence of Na^+, the EIE is estimated to be significantly >1.0. We previously determined an EIE for this process of 1.8 from direct observation of the relative concentrations of E(Aex_1) and E(A-A) and concluded that the proton abstracted from the Cα of E(Aex_1) is situated in a low-barrier H-bond in the E(A-A) complex and protected from exchange with solvent (*44*). Analysis of the free-energy reaction-coordinate diagram for stage I (see ref *55*) shows that, relative to the MVC-free species, Na^+ binding stabilizes E(Aex_1), lowers the activation energy for E(Aex_1) formation, and increases the activation energy for E(A-A) formation. The increased value of the KIE due to Na^+ binding could indicate that C−H bond scission to give E(Q_1) is more nearly complete in the Na^+-activated enzyme than in the MVC-free species (*57*, *58*).

The observed KIEs on the relaxation rate constants presented in Table 3 are respectively 2.2 ± 0.2, 2.2 ± 0.2, and 3.0 ± 0.3 for the MVC-free system, for the Na^+-bound system, and for the NH_4^+-bound system. Due to substitution of deuterium for hydrogen at Cα, the observed primary KIE on the overall, steady-state activity of the β-reaction is large for the Na^+-activated enzyme, but no significant isotope effect is detected in the MVC-free system (Table 4). The steady-state reaction in the presence of NH_4^+ demonstrated no significant primary KIE, indicating that some other step becomes rate determining for this system. Since the turnover numbers for the Na^+-, K^+-, and NH_4^+-activated enzymes are not very different, the loss of the isotope effect in the NH_4^+-activated enzyme implies that the increased efficiency of

C−H bond scission mediated by NH_4^+ is offset by a decrease in efficiency of some other step, such that the overall efficiency of turnover is not much affected.

Ammonium Ion Effects. The structures of the Na^+/K^+ sites of tryptophan synthase show ligand fields ranging from four to seven ligands depending on the ionic radius of the metal ion (*4*). The monovalent cation NH_4^+ resembles K^+ in size and charge density; thus, NH_4^+ can often replace the function of K^+. There is one important difference, however; NH_4^+ almost always bonds to MVC sites via H-bonding of the four N−H protons to four electronegative acceptor atoms to make tetrahedral or distorted tetrahedral sites. Therefore, the approximately tetrahedral geometry predicted for the NH_4^+ complex should give a structure that is more rigid than the structures of complexes formed with monovalent metal ions. The two conformations that have been identified for the MVC site of tryptophan synthase differ in the number of ligands bound to the metal ion; in the Na^+ complex, the metal ion is pentacoordinate, while the K^+ complex is tetracoordinate. Therefore, since NH_4^+ should give an obligatory tetrahedral complex, it is likely that NH_4^+ binding favors the conformation associated with a four-coordinate MVC site.

Ammonium ion binds to the metal site slightly tighter than do either K^+ or Na^+ and activates the bienzyme complex, but to a lesser extent than either metal ion (see Table 4). Interestingly, NH_4^+ is a better activator for the β-reaction, stimulating the reaction 5-fold versus 4-fold for Na^+. At equilibrium, NH_4^+ stabilizes the E(Aex_1) species in stage I of the β-reaction to a lesser extent than does Na^+ or K^+. However, the E(Aex_1) species accumulates transiently to a greater extent in the presence than in the absence of NH_4^+, just as is seen with the monovalent metal ions.

Functional Consequences of MVC Binding on Stage I. The herein reported study of MVC effects on the β-reaction pathway of the tryptophan synthase bienzyme establishes new mechanistic principles of MVC action on protein function. The tryptophan synthase example shows that the action of MVCs is the result of strong effects on two steps in the reaction pathway. Consequently, the overall effect represents a fine-tuning of catalytic activity through modulation of conformational states of the enzyme. The modulation of protein conformation alters both the activation energies and the relative ground-state energies for several steps in the pathway. A minimal mechanism incorporating these features is shown in Figure 12. The binding of Na^+ brings about an increase in the affinity of the enzyme for L-Ser, and the rate of flux through the pathway saturates at lower L-Ser (see Table 1). The rate of formation of the E(Aex_1) species is stimulated by about 3-fold in the Na^+-activated enzyme, and the affinity for L-Ser is increased about 5-fold (Table 1).

The E(A-A) species is the first intermediate on the pathway to display slow interconversion of open and closed conformations. Because the interconversion is relatively slow, the formation of E(A-A) from E(Aex_1) is the first detectable branching point in the pathway. Intermediates on the pathway prior to the E(A-A) species very likely also exist as an equilibrium of open and closed conformations. The difference is that interconversion must be relatively rapid, making the kinetic behavior of these species indistinguishable from that of a single conformation.

The available structural and solution information pertaining to the conformational states of tryptophan synthase has established that the α- and β-sites undergo conformational transitions between conformations where substrate access to the catalytic sites is unhindered and conformations where bound substrates, intermediates, and products are sequestered away from solvent (*6*). One function of the open conformation is to allow substrate binding and product release, while the closed conformations play a critically important role in preventing the escape of the channeled intermediate, indole (*6*, *41*, *42*). The catalytic competencies of the open and closed conformations have not been fully established. The available circumstantial evidence strongly indicates that the activity of the open conformation of the α-site is relatively low, and perhaps inactive (*20*). The residual α-site activity associated with the E(Ain), E(GD_1), E(GD_2), E(Aex_1), and E(Aex_2) may be due to a small fraction of the closed conformation of the α-subunit in rapid equilibrium with the open conformation. The β_2-dimer exhibits a β-reaction activity that is 50-fold less than that of the $\alpha_2\beta_2$-tetramer (*8*). Spectroscopic evidence indicates that the conformation of the β_2-dimer is similar to the open conformation of the β_2-dimeric unit of the $\alpha_2\beta_2$-tetramer (*8*, *9*). If this is the case, then it is likely that β-subunits in the open conformation also exhibit low activity, at least for some steps in the β-reaction mechanism.

This work, together with our previous studies (*2*), establishes that the positioning of the equilibrium between open and closed states plays a very important role in the $\alpha\beta$-reaction by modulating the allosteric cross-talk between the α- and β-subunits. In the β-reaction, metal ion binding shifts the rates of formation for the open and closed forms of the E(A-A) intermediate in favor of the closed form.

The changed ratio of open to closed E(A-A) species, established in stage I, is an important element of the second half-reaction (see ref *55*). Under steady-state conditions, in the MVC-free state, a significant portion of the enzyme exists as E(A-A) (*2*), and because the ratio of conformations favors the open, less active form of this intermediate, the flux takes place mainly through the less active branch. In the MVC-bound state, since most of the flux takes place through the active branch, the accumulating species is E(Aex_1), and the slowest step becomes the formation of E(A-A).

Another aspect of the change in ratio of open to closed forms involves the importance of these conformational changes to the allosteric interaction between subunits. The formation of a closed conformation in the β-subunit helps to stabilize the closed conformation of the α-subunit−IGP complex and stimulates the rate of the α-reaction (*2*, *20*, *59*). The analysis of the ammonium ion effect suggests that the tetracoordinate conformation of the metal ion binding site is the conformation responsible for shifting the equilibrium toward the more reactive E(A-A) species. This is the conformation identified by Rhee et al. (*4*, *5*) in which the βK167−αD56 salt bridge spans the $\alpha-\beta$ subunit interface. Studies of tryptophan synthase mutants with substitutions at residues assumed to be important in the conformational transition from open to closed are now underway. These studies offer new insights about the roles played by the metal ion and the βK167−αD56 salt bridge in the transmission of allosteric signals between the α- and β-sites (Woehl, Banik, Hur, Ferrari, Bagwell, Miles, and Dunn, in preparation).

REFERENCES

1. Woehl, E. U., and Dunn, M. F. (1995) *Coord. Chem. Rev. 144*, 147−197.
2. Woehl, E. U., and Dunn, M. F. (1995) *Biochemistry 34*, 9466−9476.
3. Peracchi, A., Mozzarelli, A., and Rossi, G. L. (1995) *Biochemistry 34*, 9459−9465.
4. Rhee, S., Parris, K. D., Ahmed, S. A., Miles, E. W., and Davies, D. R. (1996) *Biochemistry 35*, 4211−4221.
5. Rhee, S., Parris, K. D., Hyde, C. C., Ahmed, S. A., Miles, E. W., and Davies, D. R. (1997) *Biochemistry 36*, 7664−7680.
6. Pan, P., Woehl, E., and Dunn, M. F. (1997) *Trends Biochem. Sci. 22*, 22−27.
7. Yanofsky, C., and Crawford. I. P. (1972) *Enzymes (3rd Ed.) 7*, 1−31.
8. Miles, E. W. (1979) *Adv. Enzymol. Relat. Areas Mol. Biol. 49*, 127−186.
9. Miles, E. W. (1995) in *Subcellular Biochemistry, Vol 24. Proteins: Structure, Function and Protein Engineering* (Biswas, B. B., and Roy, S., Eds.) pp 207−254, Plenum Press, New York.
10. Wilhelm, P., Pilz, I., Lane, A. N., and Kirschner, K. (1982) *Eur. J. Biochem. 129*, 51−56.
11. Lane, A. N., and Kirschner, K. (1983) *Eur. J. Biochem. 129*, 571−582.
12. Hyde, C. C., Ahmed, S. A., Padlan, E. A., Miles, E. W., and Davies, D. R. (1988) *J. Biol. Chem. 263*, 17857−17871.
13. Hyde, C. C., and Miles, E. W. (1990) *Biotechnology 8*, 27−32.
14. Dunn, M. F., Aguilar, V., Drewe, W. F., Jr., Houben, K., Robustell, B., and Roy, M. (1987) *Indian J. Biochem. Biophys. 24*, 44−51.
15. Dunn, M. F., Roy, M., Robustell, B., and Aguilar, V. (1987) in *Proceedings of the 1987 International Congress on Chemical and Biological Aspects of Vitamin B6 Catalysis* (Korpela, T., and Christen, P., Eds.) pp 171−181, Birkhauser Verlag, Basel, Switzerland.
16. Dunn, M. F., Aguilar, V., Brzovic, P. S., Drewe, W. F., Jr., Houben, D. F., Leja, C. A., and Roy, M. (1990) *Biochemistry 29*, 8598−8607.
17. Kirschner, K., Lane, A. N., and Strasser, A. W. M. (1991) *Biochemistry 30*, 472−478.
18. Lane, A. N., and Kirschner, K. (1991) *Biochemistry 30*, 479−484.
19. Anderson, K. S., Miles, E. W., and Johnson, K. A. (1991) *J. Biol. Chem. 266*, 8020−8033.
20. Brzovic, P. S., Ngo, K., and Dunn, M. F. (1992) *Biochemistry 31*, 3831−3839.
21. Kirschner, K., Weischet, W., and Wiskocil, R. L. (1975) in *Protein−Ligand Interactions* (Sund, H., and Blaver, G., Eds.) pp 27−44, Walter de Gruyter, Berlin.
22. Houben, K. F., and Dunn, M. F. (1990) *Biochemistry 29*, 2421−2429.
23. Dunn, M. F., Brzovic, P. S., Leja, C. A., Pan, P., and Woehl, E. U. (1994) in *Biochemistry of Vitamin B6 and PQQ* (Marino, G., Sannia, G., and Bossa, F., Eds.) pp 119−124, Birkhauser Verlag, Basel, Switzerland.
24. Leja, C. A., Woehl, E. U., and Dunn, M. F. (1995) *Biochemistry 34*, 6552−6561.
25. Pan, P., and Dunn, M. F. (1996) *Biochemistry 35*, 5002−5013.
26. Kawasaki, H., Bauerle, R., Zon, G., Ahmed, S., and Miles, E. W. (1987) *J. Biol. Chem. 262*, 10678−10683.
27. Miles, E. W., Bauerle, R., and Ahmed, S. A. (1987) *Methods Enzymol. 142*, 398−414.
28. Miles, E. W., Kawasaki, H., Ahmed, S. A., Morita, H., and Nagata, S. (1989) *J. Biol. Chem. 264*, 6280−6287.
29. Yang, L. H., Ahmed, S. A., and Miles, E. W. (1996) *Protein Expression Purif. 8*, 126−136.
30. Weischet, W. O., and Kirschner, K. (1976) *Eur. J. Biochem. 65*, 365−373.
31. Dunn, M. F., Bernhard, S. A., Anderson, D., Copeland, A., Morris, R. G., and Roque, J.-P. (1979) *Biochemistry 18*, 2346−2354.
32. Koerber, S. C., MacGibbon, A. K. H., Dietrich, H., Zeppezauer, M., and Dunn, M. F. (1983) *Biochemistry 22*, 3424−3431.
33. Drewe, W. F., Jr., and Dunn, M. F. (1985) *Biochemistry 24*, 3977−3987.
34. Drewe, W. F., Jr., and Dunn, M. F. (1986) *Biochemistry 25*, 2494−2501.
35. Brzovic, P. S., and Dunn, M. F. (1994) in *Methods of Biochemical Analysis* (Suelter, C. H., Ed.) Vol. 37, pp 191−273, Wiley and Sons, New York.
36. Brzovic, P. S., and Dunn, M. F. (1995) in *Methods in Enzymology* (Sauer, K., Ed.) Vol. 246, pp 168−201, Academic Press, New York.
37. Milescu, L., Informatics Laboratory, National Institute of Biotechnology, Bucharest, Romania (http://www.bth.ro/depart/computer/orin/kinetic.htm).
38. Lane, A. N., and Kirschner, K. (1981) *Eur. J. Biochem. 120*, 379−387.
39. Lane, A. N., and Kirschner, K. (1983) *Eur. J. Biochem. 129*, 561−570.
40. Bernasconi, C. (1976) in *Relaxation Kinetics*, pp 42−45, Academic Press, New York.
41. Brzovic, P. S., Sawa, Y., Hyde, C. C., Miles, E. W., and Dunn, M. F. (1992) *J. Biol. Chem. 267*, 13028−13038.
42. Brzovic, P. S., Kayastha, A. M., Miles, E. W., and Dunn, M. F. (1992) *Biochemistry 31*, 1180−1190.
43. Miles, E. W., and McPhie, P. (1974) *J. Biol. Chem. 249*, 2852−2857.
44. Hur, O., Leja, C., and Dunn, M. F. (1996) *Biochemistry 35*, 7378−7386.
45. Evans, H. J., and Sorger, G. J. (1966) *Annu. Rev. Plant Physiol. 17*, 47−76.
46. Suelter, C. H. (1970) *Science 168*, 789−795.
47. Suelter, C. H. (1974) in *Metal Ions in Biological Systems*, Marcel Dekker, New York.
48. Larson, T. M., Laughlin, L. T., Holden, H. M., Rayment, I., and Reed, G. H. (1994) *Biochemistry 33*, 6301−6309.
49. Wells, C. M., and Di Cera, E. (1992) *Biochemistry 31*, 11721−11730.
50. Yifrach, O., and Horovitz, A. (1994) *J. Mol. Biol. 243*, 397−401.
51. Toney, M. D., Hohenester, E., Keller, J. W., and Jansonius, J. N. (1995) *J. Mol. Biol. 245*, 151−179.
52. Rhee, S., Miles, E. W., and Davies, D. R. (1998) *J. Biol. Chem. 273*, 8553−8555.
53. Schneider, T. R., Gerhardt, E., Lee, M., Liang, P.-H., Anderson, K. S., and Schlichting, I. (1998) *Biochemistry 37*, 5394−5406.
54. Brzovic, P. S., Hyde, C. C., Miles, E. W., and Dunn, M. F. (1993) *Biochemistry 32*, 10404−10413.
55. Woehl, E., and Dunn, M. F. (1999) *Biochemistry 38*, 7131−7141.
56. McDowell, L. M., Lee, M., Schaefer, J., and Anderson, K. S. (1995) *J. Am. Chem. Soc. 117*, 12352−12353.
57. Schowen, R. L. (1988) in *Mechanistic Principles of Enzyme Activity* (Libman, J. F., and Greenburg, A., Eds.) pp 119−168, VCH Publishers, Inc., New York.
58. Westheimer, F. H. (1961) *Chem. Rev. 61*, 265−273.
59. Brzovic, P. S., Miles, E. W., and Dunn, M. F. (1991) in *Proceedings of the 8th International Congress on Vitamin B6 and Carbonyl Catalysis* (Wada, H., Soda, K., Fukui, T., and Kagamiyama, H., Eds.) Pergamon Press, New York.

BI982918X